Theoretical understanding of the penetration of O2 in enzymatic redox polymer films: case of unidirectional catalysis and irreversible inactivation in a film of arbitrary thickness

Vincent Fourmond, Christophe Léger

Theoretical understanding of the penetration of O_2 in enzymatic redox polymer films: the case of unidirectional catalysis and irreversible inactivation in a film of arbitrary thickness

Vincent Fourmond[*a], Christophe Léger[a]

[a]*CNRS, Aix-Marseille Université, BIP UMR 7281, Institut de microbiologie de la Méditerranée, and Institut Microbiologie, Bioénergies et Biotechnologie, 31 chemin J. Aiguier, F-13402 Marseille cedex 20, France*

Abstract

Redox catalysts, including hydrogenases, can be embedded into films made of redox polymers, whose side chains mediate electrons between the catalyst and an electrode. These films can be used as bioanodes in H_2-based biofuel cells, because they protect the catalyst from O_2-induced inactivation: self-protection occurs because a fraction of the incoming H_2 is used in the outer region of the film to catalytically produce electrons that reduce the O_2 molecules that penetrate the film. Here, we focus on the case of unidirectional catalysis (e.g. H_2 oxidation) by an enzyme that is irreversibly inactivated by O_2, embedded in a film of arbitrary thickness. We analytically solve the reaction/diffusion system to fully describe the time evolution of the penetration of O_2 and we discuss the amount of H_2 consumed by the protection mechanism. We establish the relation between film thickness, electron conduction, catalyst use and life time. This provides the theoretical framework required to optimize the design of these systems.

Keywords: bioelectrochemistry, redox hydrogels, reaction-diffusion system, protection against O_2, catalysis

1. Introduction

Redox polymers, which bear redox side chains that can act as mediators, have a wide variety of possible applications[1], including batteries, biosensors, electrodes of biofuel cells. Redox hydrogels are hydrated films of redox polymers[2–4], which are particularly attractive for medical and/or biotechnological applications, since they are bio compatible and can host enzymes, including hydrogenases [5–7] (the enzymes that oxidize H_2[8, 9]), laccases[10, 11] (for O_2 reduction), or formate dehydrogenases[12] (which convert CO_2 to formate). When the enzyme film is deposited onto an electrode surface, mediated electron transfer occurs by hopping, that is electron transfer from one redox side chain moiety to its neighbours; this is modelled as a diffusion process.

The use of redox hydrogels took a significant step forward when Plumeré and coworkers showed that these films protect O_2-sensitive catalysts like hydrogenases[13]. This approach has since been extended to a number of other O_2-sensitive catalysts[14, 15].

This research field is developing into two different directions. First, important experimental advances have been made, including the design of new polymers or dendrimers that can accommodate various catalysts[14] or mediate bidirectional catalysis[16], and methods for obtaining homogeneous films of controlled thickness[17]. Second, the optimisation of the films also requires a better theoretical framework for understanding and predicting the catalytic current and the effects of O_2.

Regarding anaerobic systems, unidirectional catalysis by an enzyme embedded in a redox film of arbitrary thickness was explored theoretically by Andrieux and coworkers[18] and then by Bartlett and Pratt, who showed that the properties of the film depend on 3 dimensionless parameters and derived the equations for the steady-state current and concentration profiles in all 7 possible limiting cases [19]. Only three out of the 7 limiting cases are relevant in the experimental situations we are interested in. These regimes have been called V, VII and III. All other parameters being equal, the system transitions from regime V to VII and then III as the thickness of the film increases. Regimes V and VII correspond to thin and intermediate films, in which the current is limited by the catalytic reaction and by the diffusion of electrons, respectively (see the corresponding concentration profiles in fig 2). Regime III corresponds to the case of thicker films, in which the current is limited by the diffusion of both the substrate (H_2 in the case that we consider) and electrons. Regime III is not desirable for applications, since in that situation, only a tiny fraction of the catalyst is actually used for catalysis, and the limitations by the transport decrease the current. We will therefore not consider regime III further here.

Including the reactions of the enzyme and the mediator with O_2 in the reaction/diffusion kinetic model greatly complicates the system. Adding several dimensionless parameters makes the full exploration of the parameter space unfeasible, but the relevant situations can be investigated.

We have described the effect that O_2 has on films in regime III in ref. 20. We demonstrated that the protection mechanism is based on the possibility for reduced redox moieties of the

[*]To whom correspondance should be addressed. *Email address:* vincent.fourmond@imm.cnrs.fr, *Phone:* +33 4 91 16 45 36

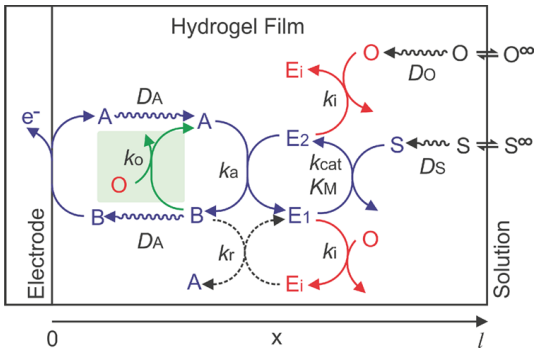

Figure 1: Schematic representation of the reactions in the hydrogel film. Reprinted with permission from ref. 20. Copyright 2015 American Chemical Society.

film to react with O_2. In the case of films embedding hydrogenases, for instance, upon exposure to O_2, a fraction of the incoming H_2 is oxidized near the outer edge of the film to provide reductive equivalents for the reduction of O_2[20] to water[21].

A combined theoretical and experimental effort made it possible to observe and explain why thinner films (in regimes VII) combine excellent catalyst use, current, and long-lasting protection[22].

In this article, we continue this theoretical investigation by focusing on the thinner films, in regimes V and VII. Their behaviour is more complex than that of the thick films in regime III because the reaction layers are not restricted to very narrow regions. We have calculated in ref. 22 the concentration profiles just after the beginning of the exposure to O_2. Here we describe the behavior of the system for an arbitrary long penetration of O_2 and derive a formula that fully describes its evolution until the film eventually collapses, when all the catalyst molecules have been inactivated by O_2.

We develop a thorough theoretical understanding of the interplay between O_2 and redox polymer films. In particular, we emphasize the existence of intrinsic limitations to the resistance, the evolution over time beyond the initial transients, and we estimate the amount of H_2 (and O_2) consumed by the protection mechanism.

2. Theoretical results

The model. We used the same model as in our previous paper[20]. Figure 1 shows a schematic representation of the film. The enzyme E is immobilized. Its substrate S (e.g. H_2) and inhibitor O (oxygen) diffuse freely within the film. The redox mediator itself is immobilized, but electrons diffuse via hopping, so that the concentrations of oxidized (A) and reduced (B) mediator also follow a usual diffusion equation, with a diffusion coefficient D_A. Like in our previous works, we assume that proton diffusion is faster than the susbtrate diffusion, to the point it is not necessary to take it into consideration. The reduced enzyme (E_2) reacts with the oxidized mediator, and the oxidized enzyme (E_1) reacts with the substrate. Oxygen reacts with the reduced mediator, and inhibits the enzyme regardless of its oxidation state. All reactions are unidirectional and have a stoechiometry of one electron. The reactions that occur in the film are:

$$\mathrm{E_2 + A \xrightarrow{k_a} E_1 + B} \qquad \mathrm{E_1 + S \xrightarrow{k_{cat}/(K_M+S)} E_2} \tag{1a}$$

$$\mathrm{B + O \xrightarrow{k_o} A} \qquad \mathrm{E_1 + O \xrightarrow{k_i} E_i} \tag{1b}$$

$$\mathrm{E_2 + O \xrightarrow{k_i} E_i} \tag{1c}$$

in which k_a is the bimolecular rate of reaction between the oxidized mediator and the enzyme, k_{cat} the maximal turnover rate of the enzyme, K_M its Michaelis constant, k_o the bimolecular rate of consumption of oxygen by the reduced mediator, and k_i the bimolecular rate of inhibition of the enzyme by oxygen. In addition to these parameters, the system is characterized by the total concentration of mediator A^Σ, the total concentration of immobilized enzyme E^Σ, the concentrations of substrate and oxygen at the outer boundary (S^∞ and O^∞), the diffusion coefficients of the mediator (D_A), of the substrate (D_S) and of oxygen (D_O), and the thickness of the film ℓ.

As before[20, 22], we used a dimensionless expression of the problem using the following variables:

$$a = \frac{\mathrm{A}}{\mathrm{A}^\Sigma} \qquad b = \frac{\mathrm{B}}{\mathrm{A}^\Sigma} \qquad e_1 = \frac{\mathrm{E_1}}{\mathrm{A}^\Sigma} \tag{2a}$$

$$e_2 = \frac{\mathrm{E_2}}{\mathrm{A}^\Sigma} \qquad e_i = \frac{\mathrm{E_i}}{\mathrm{A}^\Sigma} \qquad o = \frac{\mathrm{O}}{\mathrm{A}^\Sigma} \tag{2b}$$

$$s = \frac{\mathrm{S}}{\mathrm{A}^\Sigma} \qquad \xi = \frac{x}{\ell} \qquad \tau = k_a \mathrm{E}^\Sigma\, t \tag{2c}$$

With the additional assumptions that the active forms of the enzyme (E_1 and E_2) are at steady-state ($e_a = e_1 + e_2$ is the concentration of active enzyme, $\epsilon = e_a + e_i$), and that no significant amount of O_2 is consumed by the inactivation of the enzyme, the system can be simplified to the following set of coupled non-linear partial differential equations:

$$\frac{\partial e_a}{\partial \tau} = -\kappa_i\, o e_a \tag{3a}$$

$$\frac{\partial a}{\partial \tau} = \frac{1}{\kappa^2}\frac{\partial^2 a}{\partial \xi^2} + \kappa_o\,(1-a)\,o - \frac{e_a\, a\, s}{\epsilon(a\alpha(1+\mu s)+s)} \tag{3b}$$

$$\frac{\partial s}{\partial \tau} = \frac{\delta_S}{\kappa^2}\frac{\partial^2 s}{\partial \xi^2} - \frac{e_a\, a\, s}{\epsilon(a\alpha(1+\mu s)+s)} \tag{3c}$$

$$\frac{\partial o}{\partial \tau} = \frac{\delta_O}{\kappa^2}\frac{\partial^2 o}{\partial \xi^2} - \kappa_o\,(1-a)\;o \tag{3d}$$

in which we have introduced the dimensionless parameters defined in table 1.

Anaerobic concentration profiles. The coupled equations (3) cannot be solved analytically, but it is possible to derive approximate solutions under certain conditions. Bartlett and Pratt fully explored the parameter space in the absence of oxygen (i.e $\kappa_o = 0$ and $\kappa_i = 0$) and demonstrated that, depending on the values of the parameters, the steady-state behaviour of the film can be categorized into 7 different regimes[19].

In the present work, we only concentrate on the anaerobic regimes designated as V and VII by Bartlett and Pratt[19].

Parameter	Definition	Value
κ	$\ell\sqrt{\frac{k_a \mathrm{E}^\Sigma}{D_\mathrm{A}}}$	5–13
μ	$\frac{\mathrm{A}^\Sigma}{K_M}$	20000
ϵ	$\frac{\mathrm{E}^\Sigma}{\mathrm{A}^\Sigma}$	0.003
κ_i	$k_i \frac{\mathrm{A}^\Sigma}{k_a \mathrm{E}^\Sigma}$	585
κ_o	$k_o \frac{\mathrm{A}^\Sigma}{k_a \mathrm{E}^\Sigma}$	25000
δ_s	$\frac{D_S}{D_A}$	4000
δ_o	$\frac{D_O}{D_A}$	1000
α	$\frac{k_a K_M}{k_\mathrm{cat}}$	0.00025
o^∞	$\mathrm{O}^\infty/\mathrm{A}^\Sigma$	0.0005
s^∞	$\mathrm{S}^\infty/\mathrm{A}^\Sigma$	0.0095

Table 1: Dimensionless parameters describing the system, along with the values used in the simulations.

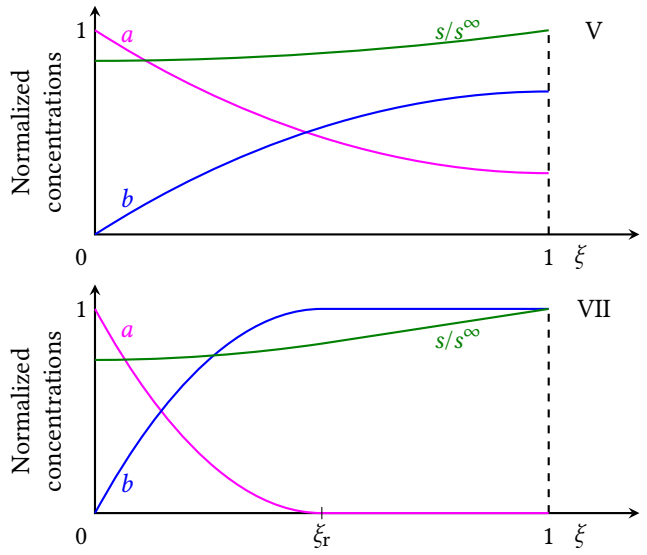

Figure 2: Schematic, normalized, anaerobic concentration profiles for the various catalytic regimes discussed in this article. The green lines correspond to concentrations of H_2, the purple ones to oxidized mediator and the blue ones to reduced mediator. The top corresponds to regime V while the bottom to regime VII. In regime VII, the value of $\xi = \xi_\mathrm{r}$ defined in equation (4) is indicated; for regime V it is not because it is larger than 1. The outer side of the film is at $\xi = 1$. The concentrations of mediator (resp. H_2) are normalized by A^Σ, the total concentration of mediator (resp. S^∞, the concentration of H_2 outside the film).

Their anaerobic concentration profiles are shown in figure 2. They are characterized by a constant production of reduced mediator in all the regions in which the film is not fully reduced ($a > 0$), due to the combination of only moderate depletion of H_2, and concentration of mediator in the film remaining greater than the Michaelis constant for the oxidized mediator. This results in *parabolic* (rather than exponential) concentration profiles. In regime V, the parabola extends across the whole film, whereas in regime VII, it extends only up to a certain position ξ_r (figure 2, bottom), whose value is (see supplementary section S2):

Regime	Current density
III	$F\left(D_A A^\Sigma + D_s \mathrm{S}^\infty\right)/\ell$
V	$F\ell E^\Sigma k_\mathrm{cat}\mathrm{S}^\infty/(\mathrm{S}^\infty + K_M)$
VII	$F\sqrt{2\,D_A A^\Sigma E^\Sigma k_\mathrm{cat}\mathrm{S}^\infty/(\mathrm{S}^\infty + K_M)}$

Table 2: Dimensional values of the anaerobic current densities predicted for regimes III, V and VII, adapted from ref. 19.

$$\xi_\mathrm{r} = \frac{1}{\kappa}\sqrt{\frac{2\,\alpha\,(1+\mu s)}{s}} \tag{4}$$

Note that ξ_r is inversely proportional to κ, which is proportional to the thickness of the film, ℓ; therefore, all other parameters being equal, changing the thickness of the film has the inverse effect on ξ_r. The transition between regime V and VII corresponds to $\xi_\mathrm{r} = 1$.

The concentration profiles in the reaction layers, where $a > 0$, are solutions of the differential equation:

$$\frac{\mathrm{d}^2 a}{\mathrm{d}\xi^2} = \frac{2}{{\xi_\mathrm{r}}^2} \tag{5}$$

This equation is mathematically equivalent from taking the limit $a \longrightarrow \infty$ in equation (3b), and assuming that s is constant in the film. In this article, we assume that the transition between the parabolic profile given by integrating (5) and the regions in which $a = 0$ (as in figure 2, bottom) is infinitely sharp. In simulations, however, the transition is smooth, and the concentration of oxidized mediator a decreases exponentially with ξ when a is no longer saturating.

For the sake of the discussion, we include in table 2 the expression of the currents for regimes III (corresponding to even thicker films), V and VII found by Bartlett and Pratt[19].

Initial penetration of O_2. An animation of the time evolution of the concentration profiles calculated with $\kappa = 7$ is available as supplementary material. Figure 3 shows the initial, stationary anaerobic concentration profiles of the reduced and oxidized mediators (panel A) and two snapshots of concentration profiles during the initial penetration of O_2. Panel C ($\tau = 0$) shows that at even just at the beginning of the exposure to O_2, the concentration of reduced mediator has already significantly decreased in the outer edge of the film, and O_2 has already penetrated about 0.05 into the film. In a first phase, the driving force for the evolution of the film during this transient is the imbalance between the incoming flux of O_2 and the outgoing flux of reduced mediator, as can be seen from comparing the red (O_2) and blue (mediator) curves in panel D which represents the fluxes. This first phase ends when O_2 has penetrated

far enough into the film that the outgoing flux of reduced mediator compensates the incoming flux of O_2, which scales as the reciprocal of the penetration depth. The first penetration depth for which the incoming flux of O_2 is balanced by the outgoing flux of reduced mediator is denoted ξ_{x0}. This balance is visible in figure 3F, where the fluxes of reduced mediator and of O_2 have the same magnitude. The second phase is the inactivation of the enzyme in the region $\xi \leq \xi_{x0}$. With the parameters given in table 1, this phase is the slowest. We have computed before its duration (cf eq. S6.70 in ref. 22):

$$\tau_0 = \frac{2\,(\exp(1) - 1)}{\kappa_i o^\infty} \tag{6}$$

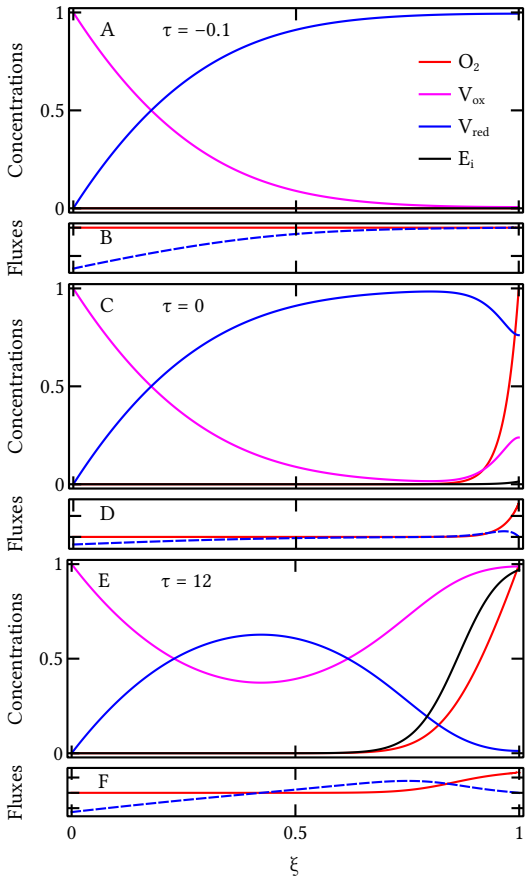

Figure 3: Concentration profiles at three times before and after exposure to O_2 of a film with a value of $\kappa = 7$ (and the other parameters given in table 1). Panels A, C and E show the normalized concentration profiles of oxidized (magenta) and reduced (blue) mediator, O_2 (red) and inactive enzyme (black). Panels B, D and F show the fluxes of reduced mediator (blue, counted positive when directed to the right) and of oxygen (red, counted positive when directed to the left). The dimensionless times with respect to the beginning of the exposure to O_2 are indicated in the panels: $\tau = -0.1$ for panels A and B, $\tau = 0$ for C and D, and $\tau = 12$ for E and F. See SI for a movie showing an animation of these concentrations profiles.

This inactivation process leads to a zone for $\xi \leq \xi_f$ for which the enzyme is inactive (ξ_f is the front of inactive enzyme). At the end of the transient, $\xi_f = \xi_{x0}$. This situation evolves afterwards, as described hereafter.

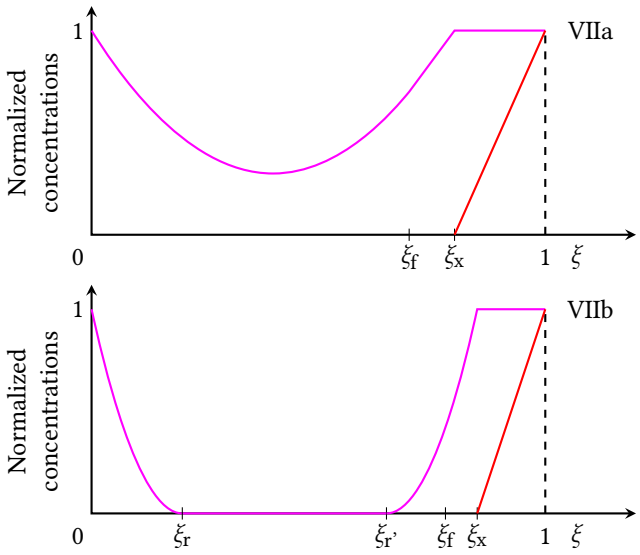

Figure 4: Schematic, normalized, aerobic concentration profiles for the two distinct cases of O_2 penetration discussed in this article. The purple lines correspond to the concentration of oxidized mediator (as in figure 2), and the red lines to O_2. The concentrations of mediator (resp. O) are normalized by A^Σ, the total concentration of mediator (resp. O^∞, the concentration of O_2 outside the film).

Aerobic profiles. After the end of the initial transient for O_2 penetration, a slowly evolving pseudo steady-state is established, in which the incoming flux of oxygen is compensated by outgoing flux of reduced mediator produced by a reaction layer on the outer side of the film. Under these conditions, the film can be divided into three distinct regions : i) for $\xi < \xi_f$, the enzyme is fully active ($e_a = \epsilon$); ii) for $\xi_f < \xi < \xi_x$, the enzyme is inactive, very little O_2 is present, so that the concentration of mediator A depends linearly on ξ; iii) for $\xi_x < \xi < 1$, the enzyme is inactive and negligible amounts of reduced mediator are present, so that the concentration profile of O_2 is linear. The values of ξ_f and ξ_x evolve over time.

Depending on film thickness, two situations can occur for $\xi < \xi_f$. In the thicker films, the two reactions layers, which produce electrons that flow towards the electrode or towards oxygen, are fully separated. This situation was referred to as "regime VIIb" in ref. 22. In thinner films, the reaction layers are merged; in particular, there is no region in which the film is fully reduced, in contrast to the VIIb case. This regime was called "VIIa" in ref. 22, but this situation also occurs with films initially in regime V. We will keep this nomenclature here.

Initial penetration depth, maximum O_2 exposure. We first consider the initial penetration depth, defined as the smallest depth for which the outgoing flux of reduced mediator compensates the incoming flux of O_2 (which equates $\delta_o o^\infty/(1-\xi_x)$). Depending on the incoming flux, the initial depth can vary greatly, and the two situations in figure 4 can occur.

We show in supplementary section S2.3 and S2.4 that the

initial penetration depth, ξ_{x0}, is given by:

$$\xi_{x0} = \begin{cases} 1 - \sqrt{1 - 2\xi_r - \delta_o o^\infty \xi_r^2} & \text{(regime VIIa)} \\ 1 - \delta_o o^\infty \, \xi_r/2 & \text{(regime VIIb)} \end{cases} \tag{7}$$

Films are in regime VIIb after the initial transient only if:

$$\xi_r < \frac{2}{4 + \delta_o o^\infty} \tag{8}$$

Else they are in regime VIIa. Note that regarding regime VIIa, equation (7) only admits a solution for:

$$\xi_r^2 \leq \frac{1}{4\,\delta_o o^\infty} \tag{9}$$

Films that do not obey this equation, i.e. very thin films, cannot produce enough electrons to counterbalance the incoming flux of O_2: they cannot be protected. For a given thickness, eq. (9) defines the maximum concentration of O_2 that a film can endure.

Concentration profiles for an arbitrary penetration in the film. Just after the initial transients, the position of the front of inactivated enzyme ξ_f equals ξ_x. As O_2 penetrates deeper and the enzyme is inactivated further in the film, ξ_f and ξ_x move away from each other, always with $\xi_f \leq \xi_x$.

We derived the full expression of the concentration of mediator for an arbitrary penetration depth (arbitrary ξ_f) in supplementary sections S2.3 and S2.4. In all cases, the profile is linear for $\xi_f \leq \xi \leq \xi_x$ and constant ($a = 1$, $b = 0$) for $\xi_x \leq \xi \leq 1$. In regime VIIa, the profile in the region $0 \leq \xi \leq \xi_f$ is parabolic. In regime VIIb, the concentration profile consists of two parabolic regions around $\xi = 0$ and $\xi = \xi_f$, separated by a region in which the mediator is fully reduced (see figure 4).

The concentration profiles are entirely determined by the values of three parameters ξ_f, ξ_r and the product $\delta^o o^\infty$. The position of the crossing point, ξ_x is given by (see supplementary section S2.3 and S2.4):

$$\xi_x = \begin{cases} \dfrac{\xi_f^2}{\xi_f^2 + \delta^o o^\infty \xi_r^2} & \text{(regime VIIa)} \\ \dfrac{2+\delta_o\, o^\infty \left(1+\xi_f - \sqrt{(1-\xi_f)^2 + \xi_r^2 (1+\delta_o\, o^\infty)}\right)}{2(1+\delta_o\, o^\infty)} & \text{(regime VIIb)} \end{cases} \tag{10}$$

The progression of O_2 in the film leads to a slow but irreversible decrease of ξ_f over time (see below).

Even if the film is initially in regime VIIb, with two separated reaction layers, as O_2 progress inside the film and ξ_f decreases, the two reaction layers eventually merge and the film enters regime VIIa. This happens when:

$$\xi_f = 1 - \sqrt{1 - 2\xi_r - \delta_o o^\infty \xi_r^2} \tag{11}$$

Further decrease of ξ_f slowly decreases the capacity of the film to consume O_2, leading to a final collapse when

$$\xi_f = \frac{1 - \sqrt{1 - 4\delta^o o^\infty \xi_r^2}}{2} \tag{12}$$

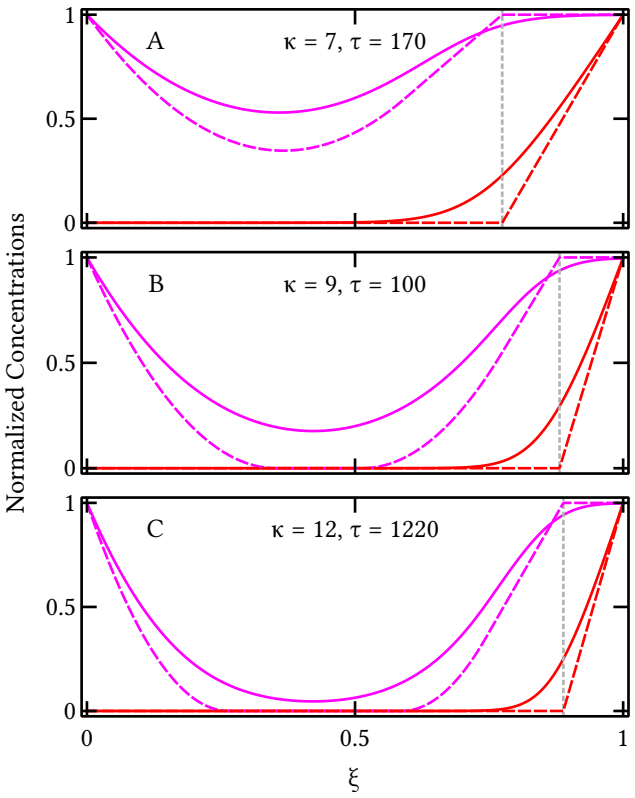

Figure 5: Comparison between simulation and prediction of the concentration profiles for different values of κ: 7, 9 and 12 respectively for panels A, B and C. The concentrations of oxidized mediator is shown in red, the concentration of O_2 is shown in blue. The solid lines are the concentrations determined from the simulations, the dashed lines are the predictions. The concentrations are normalized by A^Σ for the mediator and o^∞ for O_2. The vertical dotted lines indicate the position of ξ_x. The times were chosen to illustrate the various behaviors; the values of ξ_f were determined by numerically inversing equation (14), and are 0.59, 0.77, and 0.74 for panels A, B and C, respectively.

Figure 5 shows simulated and predicted concentration profiles of oxidized mediator and of O_2 at chosen times for $\kappa = 7, 9, 12$. The overall features of the concentration profiles are reasonably predicted from the theoretical formulas, but the concentrations of oxidized mediator are underestimated. The reason for that is clear from the O_2 concentration profiles: the derivations are made under the assumption that the concentration of O_2 is negligible for $\xi \leq \xi_x$, but the profiles in figure 5 show that there is in fact up to 30 % O_2 at ξ_x. This larger concentration of O_2 leads to a more pronounced depletion of reduced mediator, as observed.

Time evolution. After the transient, when $\xi_f < \xi_x$, the concentration of O_2 at ξ_f is very small. However, it is never strictly 0, and as the enzyme inactivation by O_2 is irreversible, the overall quantity of active enzyme decreases over time: O_2 eventually inactivates all the enzyme molecules in the film. Here, we derive a general equation for the time evolution of the front of inactive enzymes ξ_f. The progression of the front is proportional to the concentration of O_2 at ξ_f.

In the region $\xi_f < \xi < \xi_x$, as was previously shown[20]

(see also supplementary section S3), the concentration of O_2 follows an Airy function, which corresponds to a decay (for $\xi < \xi_x$) that is similar to (actually, a bit steeper than) an exponential function. Hence, the concentration of O_2 at ξ_f decreases nearly exponentially with $\xi_x - \xi_f$. Therefore, the distance $d(\xi_f) = \xi_x - \xi_f$ is a key parameter in the evolution over time of the film.

Figure 6 shows the distance $d(\xi_f) = \xi_x - \xi_f$ as a function of ξ_f predicted from equation (10), for three values of κ. The graph reads from right to left, as the value of ξ_f decreases over time. The case of $\kappa = 7$ corresponds to a film that is always in regime VIIa for all values of ξ_f. In this case, the curve resembles a parabola, going from 0 at $\xi_f = \xi_{x0}$ to a maximum at $\xi_f \approx 1/2$, and finally back to 0 at $\xi_f \approx 0.1$. The other two examples correspond to films that start initially in regime VIIb and end up in regime VIIa. In both cases, the distance is linear at high values of ξ_f, and falls back to the almost-parabolic profile described above, when ξ_f becomes smaller than the transition value given in equation (11). The profiles for $\kappa = 9$ and $\kappa = 12$ differ in that d keeps on increasing for a while even below the VIIb/VIIa limit for $\kappa = 9$.

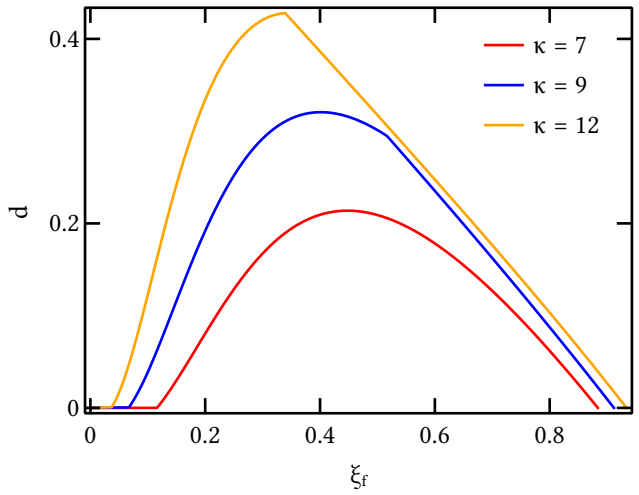

Figure 6: Distance between the front of inactive enzyme ξ_f and the mediator/O_2 crossing point ξ_x as a function of ξ_f for several values of κ. The values are predicted from equations (10). This graph reads from right to left, as the values of ξ_f decrease as O_2 penetrates further in the film over time.

We show in supplementary section S3 that the time evolution of the film can be integrated to the approximate formula:

$$\ln \tau = \ln \tau_0 + \Lambda_o \times \sqrt{\frac{(d(\xi_f))^3}{1 - \xi_f - d(\xi_f)}} \qquad (13)$$

in which τ_0 is the time of the transient given by equation (6), and Λ_o is defined by:

$$\Lambda_o = \frac{2\kappa\sqrt{\kappa_o\, o^\infty}}{3} \qquad (14)$$

Equation (13) holds only on condition that d increases when ξ_f decreases. The fact that the concentration of O_2 at ξ_f behaves as a decreasing exponential of d means that the beginning of the decrease in d results in an exponential *increase* in the concentration of O_2 at ξ_f, which leads to a rapid collapse of the film. As a consequence, the lifetime of the film can be estimated from the time at which the maximum of d is reached.

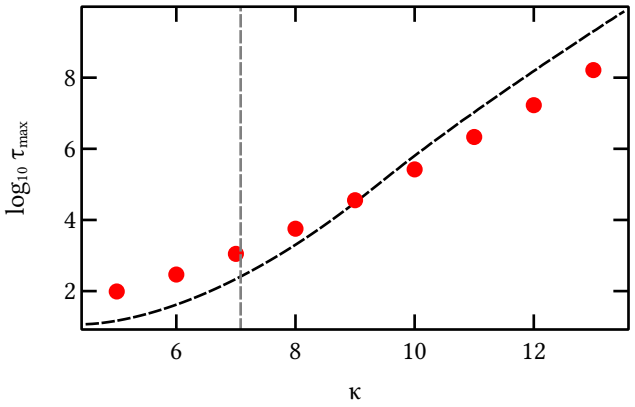

Figure 7: Lifetime of the films as a function of κ. The solid line shows the predictions derived from equations (13) and (10). The dots show the life time deduced from simulations. The vertical gray line corresponds to the limit between initial regimes VIIa and VIIb, here $\kappa = 7.08$.

Figure 7 shows the comparison between the life times predicted using equations (13) and (10) (solid line), and those determined from 9 simulations for values of κ between 5 and 13. The data show a good agreement between the prediction and the simulation, although the lifetime tends to be underestimated for low values of κ and overestimated for large values of κ.

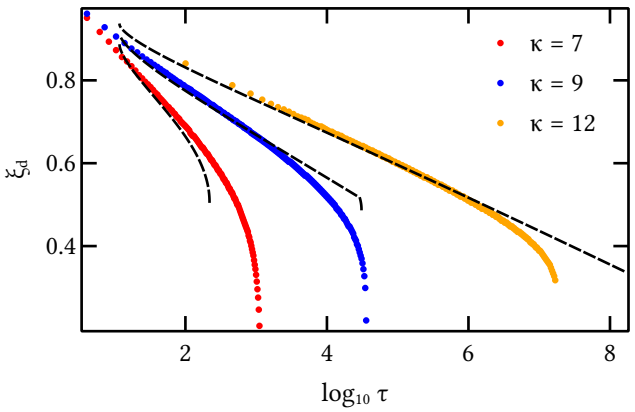

Figure 8: Evolution over time of ξ_f for several values of κ. The dots correspond to the values obtained from simulations (the values of ξ where $de_i/d\xi$ is maximum). The dashed lines show the values predicted by equations (13) and (10).

Figure 8 shows the evolution of ξ_f as a function of τ for several values of κ. The dots are the values measured from the simulation data, while the dashed lines are the values deduced from the equations. The agreement is excellent for low values of τ but less so at large times. The main difference, especially at higher values of κ, is that the predictions change much more sharply than the values deduced from the simulations. This is in line with the fact that actual concentration profiles are smoother than the predicted concentration profiles, as can be

seen in figure 5.

Consumption of O_2 – consumption of H_2 for the protection. The concentration profiles also give the quantity of O_2 (and thus H_2) consumed by the protection mechanism:

$$j_o = \frac{\delta_o o^\infty}{1 - \xi_x} \tag{15}$$

The symmetry of the concentration profiles in both thicker and thinner films just after the transient, when $\xi_x = \xi_f = \xi_{x0}$, implies that the amount of O_2 consumed is also the same as the number of electrons collected by the electrode. This flux decreases as ξ_x decreases when O_2 progresses into the film.

3. Discussion

In a previous work, we have described and characterized the concentration profiles for the case of "regime VII" films, just after the initial transient of O_2 penetration[22]. Here, we have built upon this work to derive the concentration profiles for an arbitrarily deep O_2 penetration in the film. We have obtained the stability limits of the films and we have obtained a simple expression that governs the evolution of the position of the front of inactive enzyme in the film over time, which permits the calculation of reasonably accurate life times. This contrasts with the expression proposed in ref. 22, which we based on the assumption that the linear behaviour seen at the beginning of the plot $\xi_f = f(\ln(\tau))$ (figure 8) persists until the collapse of the film.

The analytical predictions are reasonably accurate, with small deviations that are more visible in the concentration profiles than in the estimated life times. The deviations are likely due to the fact that the concentration of O_2 is assumed to be negligible below the crossing point ξ_x, where the outgoing reducing equivalents meet the incoming O_2 (figure 4). However, simulations show that the residual concentrations of O_2 at ξ_x are significant, up to 30% of the concentration outside the film (see figure 5). Another way to see the deviation is to say that we have assumed that the reaction layer between O_2 and reduced mediator is infinitely thin, whereas the simulations show otherwise.

We aim at giving insights about the parameters that need to be tuned for optimizing the resistance of the films. A remarkable fact is that the concentration profiles in the film for a given position of the front of inactive enzyme ξ_f depend on only two parameters, ξ_r and $\delta_o o^\infty$. ξ_r is the (dimensionless) length of the part of the film that contributes to the current in the anaerobic regime. $\xi_r \geq 1$ for regime V films, for which all the film contributes to the current, whereas $\xi_r \leq 1$ is the fraction of useful catalyst in regime VII films. These parameters govern the concentration profiles and also the maximum concentration of O_2 a film can sustain, given by:

$$\delta_o o^\infty = \frac{1}{4\,{\xi_r}^2} \tag{16}$$

In a dimensional form, this equation reads:

$$O^{\max} = \frac{\ell^2\, k_{\text{cat}}}{D_O\,(1 + K_M/S)} \times E^\Sigma \tag{17}$$

Hence, the only ways to increase the maximum tolerance of a film towards O_2 are to decrease the difussion coefficient of O_2 in the film, increase the film thickness, or increase the the saturating rate of production of electrons in the film under the given concentration of H_2, $k_{\text{cat}}\, E^\Sigma/(1 + K_M/S)$.

Note that this conditions does not prevent "regime V" films (for which $\xi_r > 1$) to withstand exposure to O_2, but only for values of $\delta_o o^\infty \leq 1/4$ (note that for the simulations performed in this article and also in ref. 22, the parameters from table 1 give $\delta_o o^\infty \approx 0.5$). Therefore, the nomenclature VIIa for the thinner films that we have defined in ref. 22 is not entirely appropriate; for the sake of consistence with our previous work, we have nonetheless kept it here.

Regarding the time evolution of the system, two additional parameters are relevant, Λ_o, whose expression is given by equation (14), and the duration of the transient τ_0. One can improve the resistance to O_2 of a film by decreasing ξ_r, decreasing $\delta_o o^\infty$, increasing Λ_o (eq 14) and/or increasing τ_0 (eq 6). As was previously noted[20, 22], increasing the thickness of a film improves the resistance by both decreasing ξ_r and increasing Λ_o. It was also already noted previously[20] that increasing the bimolecular rate of reaction between O_2 and the reduced mediator (κ_o) is also beneficial.

However, the fraction of catalyst used in the film is ξ_r (or 1 if $\xi_r \geq 1$), so in the interest of optimizing both the resistance to O_2 and the catalyst use, decreasing ξ_r is not an option.

The value of $\delta_o\, o^\infty$ in real units is:

$$\delta_o\, o^\infty = \frac{D_O}{D_A} \times \frac{O^\infty}{A^\Sigma} \tag{18}$$

It is probably hard to change the diffusion coefficient of O_2 within the films and the outside concentration of O_2 is often not a tunable parameter, but it is possible to increase the resistance of a given film by increasing the concentration of mediator A^Σ, or, perhaps most significantly, by increasing the diffusion coefficient of the electrons in the film.

Diffusion of electrons within the film occurs by hopping. Blauch and Savéant showed with a Monte-Carlo approach that in the case of redox moieties that are free to move around a fixed position, the apparent diffusion coefficient of the electrons can be put under the form[23]:

$$D_{\text{app}} = \frac{k \times c \times \left(\delta^2 + 3\,\lambda^2\right)}{6} \tag{19}$$

in which k is the bimolecular rate of electron self-exchange, c the concentration of the redox moieties, δ is the center-to-center distance at the electron transfer, and λ is the mean displacement of the redox moieties around their average position. The redox polymers that have been used so far for protection do not incorporate any flexibility, hence $\lambda = 0$, and the diffusion coefficients are in the 10^{-9} cm$^2 \cdot$ s^{-1} range. It was shown that incorporating flexible tethers can drastically increase the

diffusion coefficient of redox moeities attached to polymers, up to the 10^{-6} $cm^2 \cdot s^{-1}$ range[10, 11]. Although this was not done with viologens, and not with mediators with potentials suitable for the oxidation of hydrogen, this suggests that introducing flexibility in the fixation of the viologen moieties to the polymer could greatly increase the diffusion coefficient, and hence enhance the resistance to O_2, by decreasing δ_o.

However, the effect of changing the diffusion is more complex to assess than what equation (18) suggests, since ξ_r, which is a key parameter in the resistance against O_2, is proportional to ${D_A}^{1/2}$ (see equation (4) and table 1). To help the reader understand the effect, we have plotted in figure 9 a 2D plot of the predicted life time of the films by varying the diffusion coefficient of the electrons in the film between 10^{-9} and 10^{-7} $cm^2.s^{-1}$ and the film thickness between 1 and 30 µm. The data shows that, for the range of film thickness that we have investigated before[22], a diffusion coefficient of 10^{-8} $cm^2.s^{-1}$ corresponds to the optimum in terms of life time. However, the data also suggests that increasing both the diffusion coefficient and, to a lesser extent, the film thickness, could yield films with over 30% catalyst use and life times during exposures to O_2 lasting years. This is all the more desirable that, in regime VII films, the absolute magnitude of the (anaerobic) current scales as the square root of the diffusion coefficient. By increasing the diffusion coefficient and only slightly increasing the thickness, it is possible to increase both the current and the catalyst use while keeping the protection life time very high and only slightly increasing the total cost in catalyst (which is proportional to the film thickness).

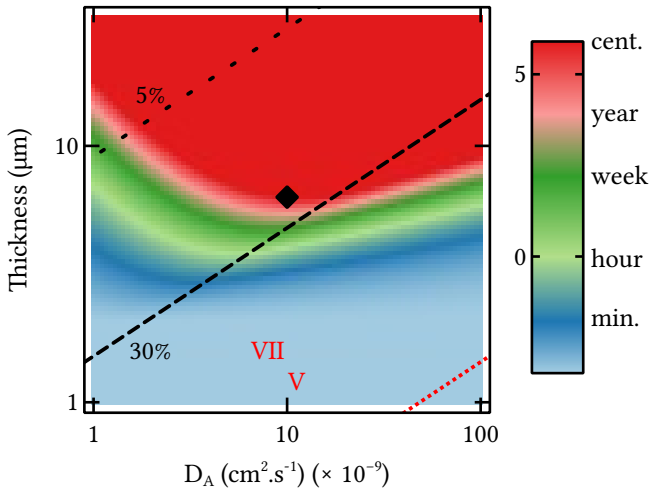

Figure 9: 2D plot of the lifetime of the film as a function of the diffusion coefficient of the electrons in the film and of the film thickness. The color corresponds to the $\log_{10}$ of the life time, expressed in hours. The legend on the side indicates which color corresponds to a lifetime of 1 minute, 1 hour, 1 week, 1 year and 1 century. The dashed and dotted oblique lines indicate the regions with 30% and 5% catalyst use under anaerobic conditions (the catalyst use increases from the top left corner to the bottom right corner of the plot). The dotted red line indicates the transition between the anerobic regimes V and VII. The diamond corresponds to the "intermediate", 6 μm film whose behavior is described in figs 2B and 4 of ref. 22.

We have also computed the incoming flux of O_2 that is consumed by the protection process, which, just after the end of the transient, corresponds also to the flux of electrons collected at the electrode, and decreases slowly as O_2 penetrates in the film. It may seem counter-intuitive that the amount of O_2 consumed is of the same order of magnitude as that of H_2 consumed in the absence of O_2, regardless of the concentration of O_2 outside of the film (in the present article, we have assumed a ratio of concentration of 19). This stems from the hypothesis that the concentration outside the film is maintained constant by fast transport (like the use of a rotating disc electrode). In practice, this very high consumption of O_2 may afford an even greater protection by depleting O_2 in the vicinity of the film.

4. Summary

We have considered the penetration of O_2 in an enzymatic redox hydrogel electrode. We have provided analytical expressions for the concentration profiles inside the film for an arbitrary penetration of O_2, and an analytical solution to the time evolution of the front of inactive enzyme within the film.

5. Methods

The system of four differential equations was solved analytically (see hereafter and Supporting Information, eq S5) or numerically using an in-house program that uses an implicit finite difference method, fourth order in time and first order in space. The numerical data sets were handled with the data analysis QSoas[24], available at `qsoas.org`, to obtain the simulation data shown in figures 7 and 8. We provide as supplementary materials the scripts that were used to compute the analytical concentration profiles and life times plotted in figures 5, 7 and 9.

Supplementary Materials

Full derivation of equations (7), (9), (7), (13) and (14); QSoas scripts for computing the life times; movie representing the initial penetration of O_2 in the film, an animated version of figure 3.

Acknowledgements

The authors acknowledge support from CNRS, Aix-Marseille Université, Agence Nationale de la Recherche (ANR-15-CE05-0020, ANR-17-CE11-002), and the Excellence Initiative of Aix-Marseille University - A*MIDEX, a French "Investissements d'Avenir" programme (ANR-11-IDEX-0001-02), and the ANR-DFG project SHIELDS (PL 746/2-1). They are part of FrenchBIC (`frenchbic.cnrs.fr`).

References

[1] R. Gracia, D. Mecerreyes, *Polym. Chem.* **2013**, *4*, 2206–2214.
[2] A. Guiseppi-Elie, *Biomaterials* **2010**, *31*, 2701–2716.
[3] Z. Shi, X. Gao, M. W. Ullah, S. Li, Q. Wang, G. Yang, *Biomaterials* **2016**, *111*, 40–54.
[4] Y. Zhao, B. Liu, L. Pan, G. Yu, *Energy Environ. Sci.* **2013**, *6*, 2856–2870.
[5] L. H. Eng, M. Elmgren, P. Komlos, M. Nordling, S.-E. Lindquist, H. Y. Neujahr, *The Journal of Physical Chemistry* **1994**, *98*, 7068–7072.
[6] A. De Lacey, M. Detcheverry, J. Moiroux, C. Bourdillon, *Biotechnol. Bioeng.* **2000**, *68*, 1–10.
[7] A. A. Karyakin, D. V. Vinogradova, S. V. Morozov, E. E. Karyakina, *Electrochim. Acta* **2010**, *55*, 7696–7700.
[8] W. Lubitz, H. Ogata, O. Rüdiger, E. Reijerse, *Chem. Rev.* **2014**, *114*, 4081–4148.
[9] M. Sensi, M. del Barrio, C. Baffert, V. Fourmond, C. Léger, *Current Opinion in Electrochemistry* **2017**, *5*, 135–145.
[10] A. Heller, *Curr. Opin. Chem. Biol.* **2006**, *10*, 664–672.
[11] N. Mano, V. Soukharev, A. Heller, *J. Phys. Chem. B* **2006**, *110*, 11180–11187.
[12] M. Yuan, S. Sahin, R. Cai, S. Abdellaoui, D. P. Hickey, S. D. Minteer, R. D. Milton, *Angew. Chem. Int. Ed. Engl.* **2018**, *57*, 6582–6586.
[13] N. Plumeré, O. Rüdiger, A. A. Oughli, R. Williams, J. Vivekananthan, S. Pöller, W. Schuhmann, W. Lubitz, *Nat. Chem.* **2014**, *6*, 822–827.
[14] A. A. Oughli, F. Conzuelo, M. Winkler, T. Happe, W. Lubitz, W. Schuhmann, O. Rüdiger, N. Plumeré, *Angew. Chem. Int. Ed. Engl.* **2015**, *54*, 12329–12333.
[15] A. A. Oughli, A. Ruff, N. P. Boralugodage, P. Rodríguez-Maciá, N. Plumeré, W. Lubitz, W. J. Shaw, W. Schuhmann, O. Rüdiger, *Nat. Commun.* **2018**, *9*, 864.
[16] S. Hardt, S. Stapf, D. T. Filmon, J. A. Birrell, O. Rüdiger, V. Fourmond, C. Léger, N. Plumeré, *Nature Catalysis* **2021**, *4*, 251–258.
[17] H. Li, D. Buesen, R. Williams, J. Henig, S. Stapf, K. Mukherjee, E. Freier, W. Lubitz, M. Winkler, T. Happe, N. Plumeré, *Chem. Sci.* **2018**, *9*, 7596–7605.
[18] C. Andrieux, J. Dumas-Bouchiat, J. Savéant, *J. Electroanal. Chem. Interfacial Electrochem.* **1982**, *131*, 1–35.
[19] P. Bartlett, K. Pratt, *J. Electroanal. Chem.* **1995**, *397*, 61–78.
[20] V. Fourmond, S. Stapf, H. Li, D. Buesen, J. Birrell, O. Rüdiger, W. Lubitz, W. Schuhmann, N. Plumeré, C. Léger, *J. Am. Chem. Soc.* **2015**, *137*, 5494–5505.
[21] H. Li, U. Münchberg, A. A. Oughli, D. Buesen, W. Lubitz, E. Freier, N. Plumeré, *Nat. Commun.* **2020**, *11*, 920.
[22] H. Li, D. Buesen, S. Dementin, C. Léger, V. Fourmond, N. Plumeré, *J. Am. Chem. Soc.* **2019**, *141*, 16734–16742.
[23] D. N. Blauch, J. M. Saveant, *J. Am. Chem. Soc.* **1992**, *114*, 3323–3332.
[24] V. Fourmond, *Anal. Chem.* **2016**, *88*, 5050–5052.

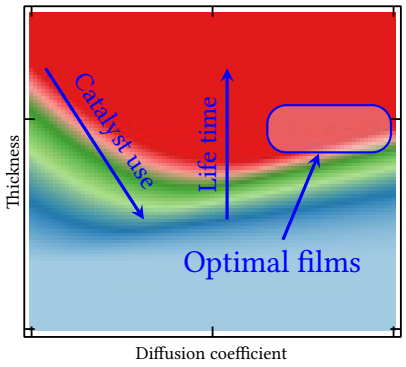

Figure 10: Graphical abstract: Embedding O_2-sensitive redox catalysts into redox hydrogels can protect them from oxidative damage. Here, we derive guidelines to help find the optimal operating conditions, combining excellent protection with excellent performance.